Coordinated Design of DIPSS and CES Using MDEA for Stability Enhancement: Jawa-Bali Indonesian Power Grid Study Case

Herlambang Setiadi[1]*   **Akbar Swandaru[2]**   **Dimas Anton Asfani[3]**
Tigor Hamonangan Nasution[4]   **Muhammad Abdillah[5]**   **Awan Uji Krismanto[6]**

[1]*Faculty of Advanced Technology and Multidiscipline, Universitas Airlangga, Surabaya, Indonesia*
[2]*ASEAN Centre for Energy, Jakarta, Indonesia*
[3]*Department of Electrical Engineering, Faculty of Intelligent Electrical and Informatics Technology, Institut Teknologi Sepuluh Nopember, Surabaya, Indonesia*
[4]*Department of Electrical Engineering, Engineering Faculty, Universitas Sumatra Utara, Medan, Indonesia*
[5]*Department of Electrical Engineering, Universitas Pertamina, Jakarta, Indonesia*
[6]*Department of Electrical Engineering, Institut Teknologi Nasional, Malangi, Indonesia*
* Corresponding author's Email: h.setiadi@stmm.unair.ac.id

Abstract: Stability of power system is one of the important keys to produce high reliability of power system. The power system must maintain the stability under small or large disturbance. However, with the increasing the load demand over the years making the power system stability is vulnerable to unstable condition when there is a disturbance. Hence adding additional controller such as dual input power system stabilizer (DIPSS) is essential. DIPSS could give a signal controller to the excitation system to produce appropriate flux when there is a disturbance emerge. However, DIPSS alone is not enough to handle the small and large disturbance as DIPSS is not directly giving a damping to the source of disturbance. Hence, adding capacitor energy storage (CES) can be solution to handle this problem. CES can give a fast active power when there is load changing. This paper proposed a coordinated design between CES dan DIPSS using modified differential evolution algorithm (MDEA). Jawa-Bali Indonesian Power Grid is used as the test system. Non-linear time domain simulation is carried out to investigate the efficacy of the proposed controller method. In addition, transient kinetic energy (TKE) assessment is carried out to investigate how much kinetic energy produced by the system. From the simulation results, it is found that the proposed method giving a better stability indicated by the smallest overshoot and the fastest settling time compared to the other scenarios. Furthermore, it is found that the proposed method controller could give a smallest TKE value (0.0000004076) compared to the other scenarios.

Keywords: CES, Clean energy technology, DIPSS, MDEA.

1. Introduction

In this era, the electrical energy consumption capacity is increasing significantly. This condition happened due to the rapid development of technology, and human growth over the year. The increasing of power plant is directly proportional with the increasing of load demand affected by rapid growth of human population. The increasing load demand as well as the power plant bring a challenge to the power system stability. One of the stability types that can be directly influenced with those condition is low frequency oscillation stability [1]. Low frequency oscillation or small signal stability of power system is the ability of power system to find their stable conditions after being subjected by small perturbation [2]. Low frequency oscillation can be classified into two different types (local and global) based on their oscillations. Generally, this problem can be simply handled by adding damper windings on the rotor of generator. However, over time the performance can deteriorated. Another way is by adding a power system stabilizer (PSS) as additional controller of

excitation system [3]. However, PSS only may not be sufficient if the system is larger and have high uncertainty. Hence additional devices such as energy storage devices can be an alternative solution for this problem.

There is a couple of energy storage types such as capacitive energy storage, ultracapacitor energy storage, superconducting magnetic energy storage, redox flow batteries, and battery energy storage system. Umer [4] studied shows that frequency performance can be enhanced by using ultracapacitor energy storage. However, in that research the application of ultracapacitor is used only for frequency regulation study. Very scant attention has been paid on investigating the impact of ultracapacitor in dynamic stability study. The application of superconducting magnetic energy storage (SMES) for load frequency control is reported in [5]. It is observed that by adding SMES the frequency performance can be enhanced significantly. Redox flow battery is also reported give significant influence on frequency performance of power system [6]. Research efforts in [7] reported that by adding BESS can be used to handle the uncertainty of PV plant. Among numerous types of energy storage capacitor energy storage (CES) is showing a significant development over the past few decades. It is reported in [8], shows the application of capacitive energy storage to regulate the frequency performance of multi-source power system. It was found the frequency performance of multi-source power system can be enhanced by adding capacitive energy storage indicated by the smallest overshoot and fastest settling time of the frequency. From reference 4 until 8 the application of energy storage is on frequency regulation. Hence it is important to investigate the impact of CES on dynamic stability. In addition, CES can provide a better result when added to the system, the problem is how to design CES parameter without jeopardizing the stability boundary. Hence, metaheuristic algorithm can be used to design CES parameter.

This paper proposed method to enhance the low frequency oscillation stability of power system by coordinated control between capacitor energy storage and dual input power system stabilizer (DIPSS). To get the better performance, the CES and DIPSS parameters are designed using modified differential evolution algorithm (MDEA) [9]. The rest of the paper is organized as follows: Chapter 2 shows the modelling of DIPSS and CES. MDEA, test system, and the procedure of coordinated control using MDEA are presented in Chapter 3. Chapter 4 shows the results and discussion of the paper. The conclusion of the paper is presented in Chapter 5.
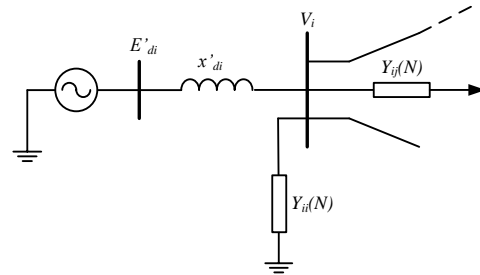
Figure. 1 Equivalent circuit of electric power system

2. Modelling

2.1 Dynamic model of power system

In this paper the power system is represented as multi-machine model. In this model, the resistance of the resistor is neglected, the condition of the system is considered balanced, the saturation of the generator core is ignored, and the load is modelled as a static load. Fig. 1 shows the multi machine system with n connection machines and the *i-th* machine connecting terminal

$Y_{ij}(N)$ is the admittance matrix element of the *ij-th* grid. E'_{qi} is the voltage of the *i-th* generator on the q-axis (quadrature). Furthermore, Vi is the voltage on the *i-th* generator bus, while $Y_{ii}(N)$ is the line-to-ground admittance of the the *i-th* bus. Moreover, x'_{di} is the d-axis (direct) transient reactance of the *i-th* generator. Therefore, the relationship between variables can be written using Eqs. (1) to (4) [10].

$$I= Y_N V \qquad (1)$$

$$E'q= V+[jx_d']I \qquad (2)$$

$$I=YE'_q \qquad (3)$$

$$Y=[Y_N^{-1} + [jx_{di}']]^{-1} \qquad (4)$$

In Eqs. (1) to (4) Y, I, Y_N and V are bus admittance matrix, current vector in the network, network admittance matrix and bus voltage vector. The value of the bus voltage on the *i-th* generator on the q-d axis is described using Eq. (5) [10].

$$V_i = V_{di} + V_{qi} \qquad (5)$$

Eq. (5) can be rewritten as linear model as described in Eqs. (6) to (8). Where, V_{di} is the d-axis generator bus voltage of the *i-th* machine. While V_{qi} is Voltage of the *i-th* machine q-axis generator bus. Furthermore, Vi is change in the *i-th* machine bus voltage, while i_{di} is the current of the d-axis of the *i-th* machine. Moreover, i_{qi} is the q-axis current of the *i-th* machine [10].

$$V_i \Delta V_i = V_{di} \Delta V_{di} + V_{qi} \Delta V_{qi} \qquad (6)$$

$$\Delta V_{di} = X_{di}{}' \Delta i_{qi} \qquad (7)$$

$$\Delta V_{qi} = \Delta E{}'_{qi} - X_i{}' \Delta i_{di} \qquad (8)$$

By substituting the current equation into Eqs. (5) to (8), the *i-th* generator bus voltage equation is obtained using Eq. (9). Eq. (9) is referred to the voltage equation on the bus in front of the *i-th* generator of the multi-machine interconnect system [10].

$$\Delta V_i = K_{5,ii}\Delta\delta_i + K_{6,ii}\Delta E_{qi} - \sum_{i\neq j} K_{5,ij}\Delta\delta_j + \sum_{i\neq j} K_{6,ij}\Delta\delta_{qi} \qquad (9)$$

Where
$$K_{5,ii} = \sum_{i\neq j} K_{5,ij} \qquad (10)$$

$$K_{6,ii} = \cos\sigma_i - x'_{di}y_{ii}\sin(\beta_i - \sigma_i) \qquad (11)$$

$$K_{5,ij} = E'_{dj}x'_{di}y_{ij}\cos(\beta_i + \delta_{ij} - \sigma_i) \qquad (12)$$

$$\delta_{ij} = \delta_i - \delta_j \qquad (13)$$

$$K_{6,ij} = x'_d y_{ij} \sin(\beta_{ii} + \delta_{ij} - \sigma_i) \qquad (14)$$

The linear model of the synchronous machine includes the torque equation model and the field equation. The relationship between the change in the power angle and the change in flux velocity can be written in the form of a differential equation as described in Eqs. (15) and (16) [10, 11].

$$\dot{\delta}_i = \omega_{0i}\Delta\omega_i \qquad (15)$$

$$\dot{\Delta\omega}_i = \frac{1}{M_i}(T_{mi} - T_{ei} - D_i\Delta\omega_i) \qquad (16)$$

The mathematical representation T_{ei} can be expressed by using Eq. (17). The parameters in Equation (17) can be described using Eqs. (18) to (21) [10, 12].

$$\Delta T_{ei} = K_{1,ii}\Delta\delta_i + K_{2,ii}\Delta E'_{qi} - \sum_{j^1 i} K_{1,ij}\Delta\delta_j - \sum_{j^1 i} K_{2,ij}\Delta E'_{qj} \qquad (17)$$

$$K_{1,ij} \neq \sum_{i\neq j} K_{1,ij} \qquad (18)$$

$$K_{2,ii} = E'_{qi}G_{ii} - \sum_{i\neq j} E'_{qi}y_{ij}\cos(\beta_{ii} + \delta_{ij})K_{1,ij} \qquad (19)$$

$$K_{1,ij} = E'_{qi}E'_{qj}y_{ij}\sin(\beta_{ij} + \delta_{ij}) \qquad (20)$$

$$K_{2,ij} = E'_{qi}E'_{qj}y_{ij}\sin(\beta_{ij} + \delta_{ij}) \qquad (21)$$

The *i-th* machine field equation in the form of a linear model can be written as Eqs. (22) and (23) [10].

$$T'_{d0i}\Delta E_{qi} = \Delta V_{FDi} - \Delta E_{qi} - (x_{di} + x'_{di})\Delta\Delta_{di} \qquad (22)$$

$$\Delta\dot{E}_{qi} = -\Delta\frac{d}{dt}E'_{qi} \qquad (23)$$

With

$$\Delta i_{di} = -\sum_{j\neq i} E'_{qi}y_{ij}\cos(\beta_{ij} + \delta_{ij})\Delta\Delta_{ij} - B_{ii}E'_{qi} - \sum_{j\neq i} y_{ij}\sin(\beta_{ij} + \delta_{ij})E'_{qj} \qquad (24)$$

B_{ii} = *i-th* machine admittance imaginary component. Substituting the equation i_{di} into Eq. (24) produces Eq. (25) [10].

$$T'_{d0i}\Delta\dot{E}_{qi} = \Delta V_{FDi} - C_{3,ii}\Delta E'_{qi} + K_{4,ii}\Delta\delta_i + \sum_{j\neq i} C_{3,ij}E'_{qj} - \sum_{j\neq i} K_{4,ij}\Delta\delta_j \qquad (25)$$

With
$$C_{3,ii} = 1 - (xi_{di} - x'_{di})B_{ii} \qquad (26)$$

$$K_{4,ii} = \sum_{j\neq i} K_{4,ij} \qquad (27)$$

$$C_{3,ij} = (xi_{di} - x'_{di})y_{ij}\sin(\beta_{ij} + \delta_{ij}) \qquad (28)$$

$$K_{4,ij} = (x_{di} - x'_{di})E'_{qi}y_{ij}\cos(\beta_{ij} + \delta_{ij}) \qquad (29)$$

In this paper the excitation system is refers to the IEEE type 1 excitation model. The mathematical representation of IEEE type 1 excitation system is described using Eqs (30) to (32) [10].

$$\Delta\dot{V}_{FDi} = \frac{\Delta V_{Ai}}{T_{Ei}} - \frac{K_{Ei}\Delta V_{FDi}}{T_{Ei}} \qquad (30)$$

$$\Delta\dot{V}_{Fi} = \frac{K_{Fi}\Delta V_{Ai}}{T_{Ei}T_{Fi}} - \frac{K_{Ei}K_{Fi}\Delta V_{FDi}}{T_{Ei}T_{Fi}} - \frac{K_{Fi}}{T_{Fi}} \qquad (31)$$

$$T_{Ai}\dot{\Delta V}_{Ai} = \Delta U_{2i}K_{Ai} - \Delta V_{Fi}K_{Ai} - \Delta V_{Ai} - V_i K_{Ai} \qquad (32)$$

The turbines used in the Java Bali 500 kV multi-machine system are water turbines and steam turbines. The water turbine has input in the form of mechanical power that comes from the thrust of water coming out of the water pipe (penstock) of the dam. In addition, this turbine has an output of mechanical power (torque) which is used to rotate the generator. Turbine also has an auxiliary controller to regulate the turbine rotation. This controller is called governor. The linear model of the water turbine and governor can simply

be formed in a linear mathematical representation as shown in Eqs. (33) and (34) [10].

$$\dot{\Delta T}_{mi} = \left(\frac{2}{T_{wi}} + \frac{2}{T_{gwi}}\right)\Delta Y_i - \frac{2K_{gwi}\Delta U_{1i}}{T_{gwi}} + \frac{2K_{gwi}\Delta \omega_i}{R_i T_{gwi}} - \frac{2\Delta T_{mi}}{T_{wi}} \tag{33}$$

$$\dot{\Delta Y}_i = \frac{K_{gwi}}{T_{gwi}}\Delta U_{1i} + \frac{K_{gwi}\Delta \omega_i}{R_i T_{gwi}} - \frac{\Delta Y_i}{T_{gwi}} \tag{34}$$

The steam turbine has input in the form of mechanical energy that is emitted from the steam boiler and has an output of mechanical energy (torque) which is used to drive the steam turbine. The steam turbine model in linear representation can be seen in Eqs. (35) and (36). In linear models, the difference between a water turbine and a steam turbine lies in their parameter values [10].

$$\dot{\Delta T}_{mi} = \left(\frac{2}{T_{ui}} + \frac{2}{T_{gui}}\right)\Delta Y_i - \frac{2K_{gui}\Delta U_{1i}}{T_{gui}} + \frac{2K_{gui}\Delta \omega_i}{R_i T_{gui}} - \frac{2\Delta T_{mi}}{T_{ui}} \tag{35}$$

$$\dot{\Delta Y}_i = \frac{K_{gui}}{T_{gui}}\Delta U_{1i} - \frac{K_{gu}\Delta \omega_i}{T_{gui}R_i} - \frac{\Delta Y_i}{T_{gui}} \tag{36}$$

2.2 Dual input power system stabilizer

The advantages of DIPSS are enhancing damping by combining two signals, rotor speed (mechanical signal) and the electrical power of the machine (electrical signal) [13]. These two signals correspond to the active power and reactive power. By detecting active and reactive power error signals, a DIPSS can provide more detail and a precise damping signal injected to the excitation system. This error signal can be derived from the shaft motion e.g. lateral shaft run-out that causes excessive modulation of the generator excitation system or it can also come from torsional oscillations resulting from electrical torque changes. This error signal component will influence the excitation of the generator and have an impact on the electrical torque. Each input signal is fed to the washout and transducer circuit. The washout circuit provides continuous conditioning at the output of the stabilizer while the transducer is used to convert the input signal into a voltage signal. A block diagram of a dual input PSS based on the IEEE type 2B is shown in Fig. 2 [14].

Each input signal will be passed into the washout block diagram and one transducer. Furthermore, both input signals will be added and passed into torque filter. A detailed description of each component in the dual-input PSS is described below: Speed signal is
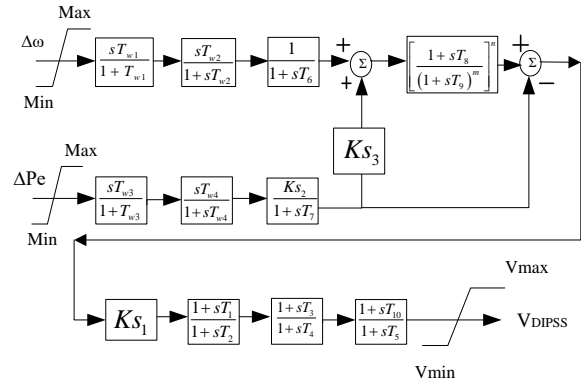
Figure. 2 Dual input power system stabilizer

generally obtained from the magnetic-probe or gearwheel on the generator. This process of obtaining the signal generally results in a noisy signal, resulting in an error in the speed signal value. In this block, the signal is passed to the high pass filter to remove the average speed level and produce signals from the speed deviations. By using this signal, the stabilizer could only change the speed instead of changing the reference from the generator terminal [15].

Generator electrical power output can be obtained from the secondary Voltage transformer and the current transformer of the generator. In this block diagram, the power signal is passed into a high pass filter to achieve the requirement. In this case through the integral and scaling stages of the signal. Mechanical power signal consists of a low pass filter and a ramp tracking filter. This filter is used to adjust the mechanical power values. The first filter is used to provide a weakening of the torsional component in the speed signal. The second filter is used for zero steady state errors.

Stabilizing signal selection and phase compensation is identical to the generic PSS block diagram. This block diagram serves as a phase lead provider on electromechanical frequency. This phase is used to compensate for the phase lag [16]. Voltage limiter is used to limit the output signal from the DIPSS so that the resulting signal is still within the safe limit to be entered into the AVR so there is no overvoltage [17].

2.3 Capacitor energy storage

Capacitor energy storage (CES) is one of the energy storage devices that can store and release large amounts of power simultaneously. CES stores energy in the form of an electric field in the capacitor. CES consists of a storage capacitor and Power Conversion System (PCS) with the control and protection [18]. Storage capacitor is composed of several discrete capacitors connected in parallel, with capacitance C.

255
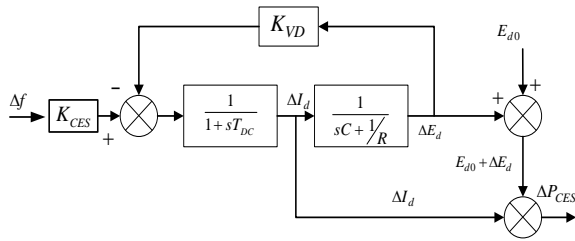
Figure. 3 CES block diagram

Losses and dielectric capacitor banks at CES are modelled by resistance R connected in parallel to the capacitor.

Storage capacitor is connected to the grid via the PCS. PCS consists of AC to DC rectifier and inverter DC to AC. Thyristor bypass is used to provide a way for current Id when converter failure emerges. In addition, DC breaker can be used to put Id current to resistor Rd when converter failures emerge.

Changes of currents direction during charge and discharge are resolved with the preparation of the switch using a gate turn off thyristors (GTO). In charging mode, switches S1 and S4 are set on and the switches S2 and S3 are set off. In the discharging mode, switches S2 and S3 are set on and S1 and S4 are set off [18]. Linear model of CES is shown in Fig 3. From Fig. 3, it can be seen that the frequency deviation (∆f) of each area of the power system is used as the input signal of CES.

3. Method

3.1 Modified differential evolutionary algorithm

The Modified Differential Evolution Algorithm (MDEA), or a form of Differential Evolution Algorithm (DEA) which has been modified, is designed with the purpose to obtain a better optimization results [19]. In this algorithm, rather than plain DEA, MDEA role is emphasized more in the process of mutation which done based on the restrictions of escalated particle displacement percentage. In addition, the increasing number of iterations is essential on the mutation process. Hence, the particle velocity of MDEA at each iteration tend to be smaller and shift particles tend to be decreased gradually. Unlike DEA, which emphasizes the similarity of the particle displacement value at each iteration. Moreover, the value of the particle velocity occurrence tends to be always fixed. Reference [20] also states that the particle velocity which occurs in the process of DEA generating particle tends in a static gap.

M.R.Nayak, Krishnanand K.R and P.K. Rout found that global optimum, along with local optimum, will be able to be distinguished by implementing

"best fitness value" at each iteration. This condition can be satistified as long as assuming the sequence of DEA that applying one unit of the best particle which consecutively did a move from a particular particle to another particle in an iteration. This condition will not be a serious problem if the global optimum position and the position of local optimum is not severely complicated. However, it would be a problem if the system parameter which to be tested are quite a lot, where it makes the position of local optimum and the global optimum in a range of multi-parameter, undoubtedly becoming more complex. This actually can be solved by applying a limitation value for the particle velocity progressively. In addition, the speed of the particle at each iteration is set so that the particle gap tends to be swarmed in areas that have the potency to become a global optimum.

MDEA implement those procedures above by manipulating the DEA mutations in such a way that it could be compromized. The mathematical representation in Eq. (37) shows how MDEA manipulated the mutation process of conventional DEA.

$$v_{i,g}(r) = x_{best}(r)\lambda + x_{r0,g}(r)(\lambda - 1) + F \times \left(x_{r1,g}(r) - x_{r2,g}(r)\right) \quad (37)$$

Where:

$$\lambda = \frac{max\_iter - r}{max\_iter} \quad (38)$$

In Eqs. (37) and (38), iteration is expressed by r. λ value here can be reduced as well as iteration passes. This meant that the best solution, $x_{best}(r)$, has a more influential role than random solutions $x_{r0,g}(r)$). Furthermore, with increasing iterations, the role of random solutions $(x_{r0,g}(r))$ the greater, in tandem with the shrinking role of the best solution $(x_{best}(r))$. The expectation of this modification is to balance the algorithm role in terms of both exploration and exploitation considering the succesive move of every particle which to be carried out. As stated before, this so called MDEA have the same sequence procedure as well as DEA [21]

MDEA use a pair of vector population with the D-dimensional parameter. Initial population, P_x, consisting of the vector $x_{i,g}$ as the initial point. The mathematical representation of initial condition of MDEA can be described using Eqs. (39) and (40) [22].

$$P_{x,g} = (x_{i,g}), \quad i = 1, ..., N_p, \quad g = 1, ..., g_{max} \quad (39)$$

$$x_{i,g} = (x_{j,i,g}), \quad j = 1, \dots, D. \qquad (40)$$

In Eqs. (39) and (40) $x_{i,g}$ is the i-th vector in the generation to g. While $x_{j,i,g}$ is the value of the i-th vector in the j-th parameter, in the generation to g. Value of i is an integer from 0 to N_p, g is an integer from 0 to g_{max}, and j is an integer from 0 to D-1 [23].

The next population, $P_{v,g}$, a population containing N_p vector-vector are mutated randomly DE $v_{i,g}$. The mathematical representation of this step can be described using Eqs. (41) and (42)

$$P_{v,g} = (v_{i,g}), \quad i=1,\dots,N_p, \quad g=1,\dots,g_{max} \qquad (41)$$

$$v_{i,g} = (v_{j,i,g}), \quad j = 1, \dots, D - 1. \qquad (42)$$

Then, each vector in the initial population are recombined with the mutant vector to generate a trial population, $P_{u,g}$, with N_p trial vector, $u_{i,g}$. The mathematical representation of trial population and trial vector can be described using Eqs. (43) and (44).

$$P_{u,g} = (u_{i,g}), \quad i=1,\dots,N_p, \quad g=1,\dots,g_{max} \qquad (43)$$

$$u_{i,g} = (u_{j,i,g}), \quad j = 1, \dots, D. \qquad (44)$$

In the process of recombination, mutant population was replaced by a population of trial in order to obtain a pair of populations, initial population (current population) and the trial population, that will be processed in a DE. Mutations in DE is already shown before by Equation 40. So that the sequence is slightly different from DEA. Crossover is also used by MDEA, like DEA, to form a trial vector of parameter values doubled from two different vector that is, the initial vector with the mutant vector. Crossover in DE is shown by Eq. (45).

$$\begin{cases} v_{j,i,g} \ if(rand_j(0,1) \le Cr \ or \ j = j_{rand} \\ x_{j,i,g} \ yang \ lain \end{cases} \qquad (45)$$

The probability of crossover, with a range of C_r [0,1], is the value determined by the user to control the distribution of parameter values are duplicated from the mutant. $rand_j$ (0.1) is a random value that determines whether the vector is in-crossover or not [24].

Selection is used to determine the vector which the value of the selection vector is carried out to determine the vector that will become members of the population for the next iteration. Conversely, if the trial vector, $u_{i,g}$, has the objective function value greater than the target vector $x_{i,g}$, then the target
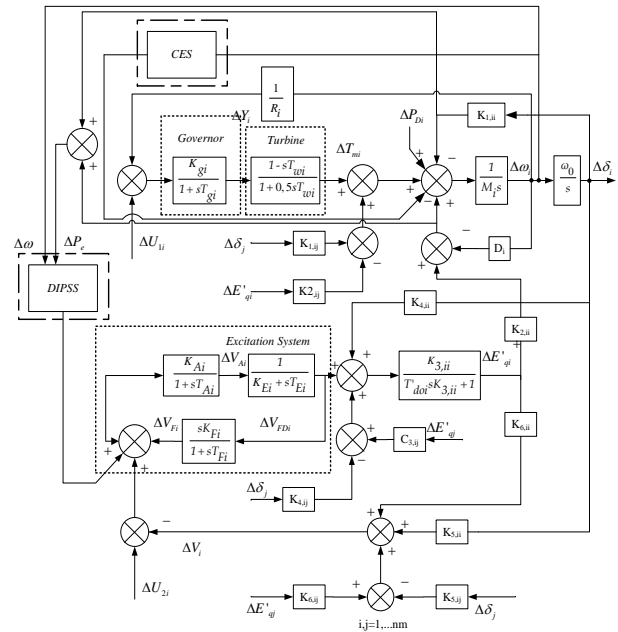
Figure. 4 CES and DIPSS installation on system

vector remains a member in the generation or the next iteration. The selection proses can be modelled as described in Eq. (46)

$$x_{i,g} = \begin{cases} u_{i,g} \ if \ f(u_{i,g}) \le f(x_{i,g}) \\ x_{j,i,g} \ others \end{cases} \qquad (46)$$

3.2 Procedure of designing the controller

In this research, DIPSS is placed in Suralaya power plant only, while CES are placed in all the eighth regions. In other word, it can be stated that this research is using one DIPSS and eight CESs. Multi-machine system with DIPSS and CES are shown in Fig. 4.

Fig. 5 shows a flowchart of DIPSS and CES controller tuned by using MDEA. Here, the objective stability of the system is to be tested by using the Comprehensive Damping Index (CDI) [25]. Here, Comprehensive Damping Index (CDI) conducted by the Eqs. (47) to (49).

$$\lambda_i = \sigma_i \pm j\omega_i \qquad (47)$$

$$\xi_i = \frac{\sigma_i}{\sqrt{\sigma_i^2 + \omega_i^2}} \qquad (48)$$

$$CDI = \sum_{i=1}^{n}(1 - \xi_i) \qquad (49)$$

The parameters of DIPSS and CES controllers were optimized by using a MDEA are performed in 300 iteration system is 12417.8 MW. Moreover, the total load of the system is 10361 MW [26].
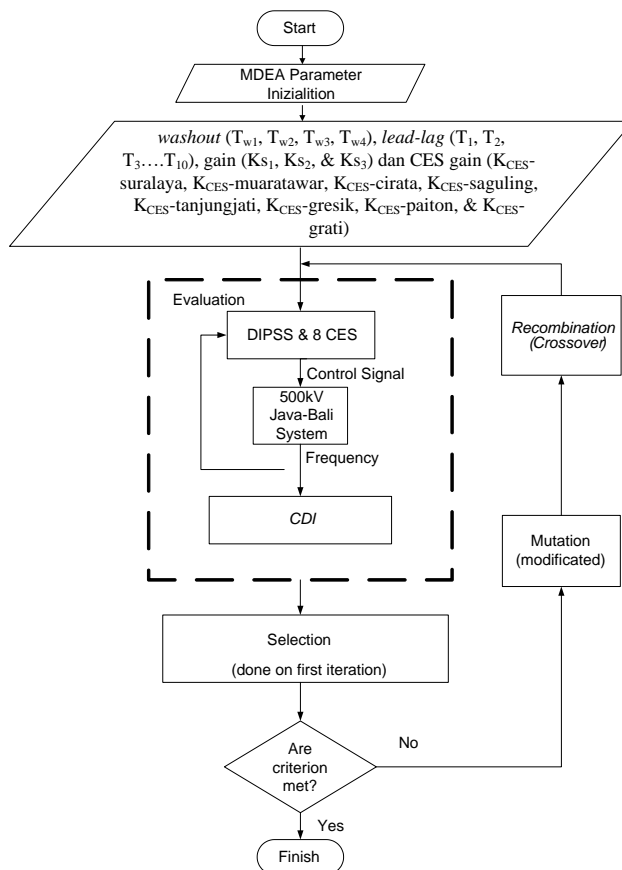
Figure. 5 Flowchart of DIPSS and CES optimization using MDEA
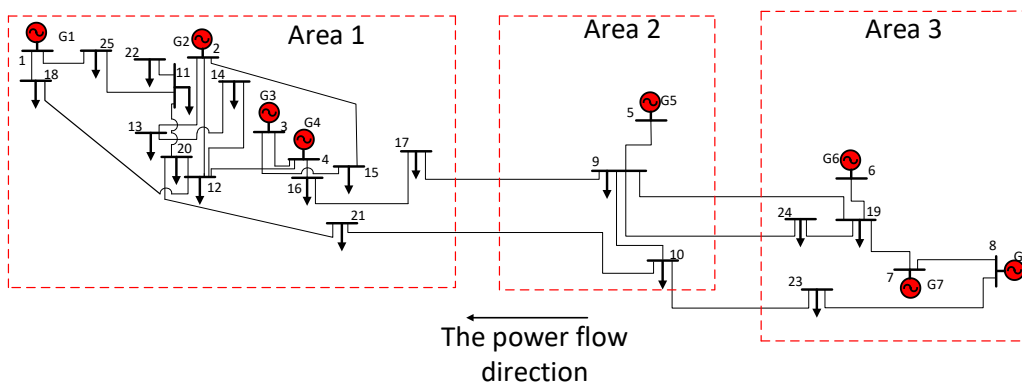
Figure. 6 Jawa-bali indonesian power grid

4. Results and discussions

A 500 kV Java Indonesia power grid is shown in Fig. 6 and is used as the test system of this paper. This system is divided into three areas connected through the high voltage long transmission line from the east side of Java Island to the west side of Java Island. The distance between area 1 and area 2 is 500 km, while the distance between area 2 and area 3 is 500 km. This system consists of 8 generator buses and 17 bus loads. The total generating and load capacity on area 1 are 4478.6 MW and 1738 MW. The total generating and load capacity on area 2 are 1321. 6 MW and 558 MW.

While the generating capacity and load in area 1 are 6201,2 and 8065 MW. The total generating capacity of this Fig. 7 shows the convergence graph of MDEA for tuning DIPSS and CES parameters. From the picture, it can be observed that the minimum value function of the system performance is obtained at iteration 289. To test the proposed method to case studies are conducted in this paper. The first case study is to investigate the non-linear time domain simulation of the system, while the second case study focused on described how much kinetic energy is produced on each scenario. Table 1 shows the scenarios used in this research to shows the efficacy
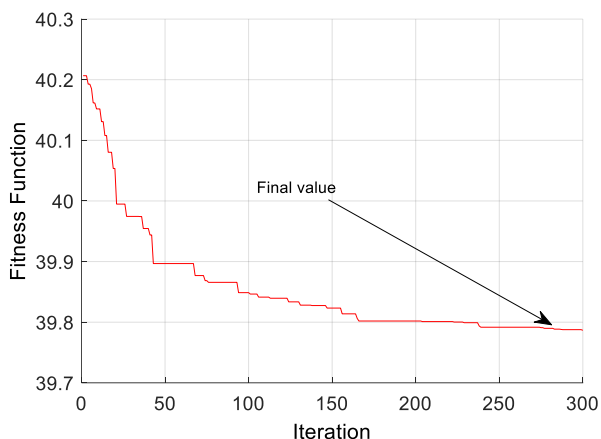
Figure. 7 Convergence graph of MDEA

Table 1. Scenarios

Scenarios	System
1	No additional controller
2	PSS DEA
3	DIPSS DEA
4	DIPSS-CES DEA
5	DIPSS-CES MDEA

of the proposed method. In this paper only Suralaya power plant response is described in the paper as the source of disturbance is on Suralaya power plant.

4.1 Case study 1

In this case study, investigation of the system non-linear response is carried out. Three different response (rotor speed, rotor angle and voltage) are thoroughly investigated the shows the efficacy of the proposed method. In order to plot the non-linear response of the investigated system, the weak mode of the system should be excited. To excite the weak mode in this system, a small perturbation of load changes in given in the Suralaya power plant. Figure 8 shows the no-linear time domain simulation of Suralaya power plant rotor speed. From the figure, it is noticeable that the best response is provided by the proposed method (Scenario 5). This is indicated by the smallest overshoot and the fastest settling time compared to the other scenarios. Table 2 illustrates the detailed features of the Fig. 7. It is noticeable that due to optimal parameter tuning by MDEA, DIPSS could provide optimal signal control to the excitation system. In addition, CES could also provide optimal damping to the system so that the overshoot can be damp as well as accelerate the settling time of the system.

Another non-linear time domain response that is essential to investigate the rotor angle transient response. Rotor angle response is indicated how the interconnected system maintain the synchronization after subjected by disturbance. The aim of the
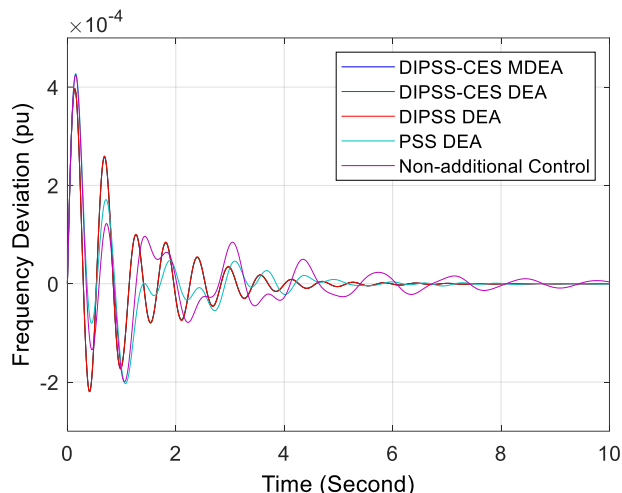
Figure. 8 Frequency response changes in Suralaya power plant

Table 2. Detailed features of Figure. 8

Index	Scenario 1	Scenario 2	Scenario 3	Scenario 4	Scenario 5
Overshoot	4.2492×10^{-4}	4.2732×10^{-4}	3.9662×10^{-4}	3.9652×10^{-4}	$3,9634 \times 10^{-4}$
Settling time	>10	8.6	7.2	7.2	7,2

proposed controller is to make the rotor angle produce a minimum overshoot. In addition, the goal of the proposed method is to get new angle position as fast as the system can manage. Figure 8 depicts the rotor angle's non-linear time domain under different scenarios. While Table 3 shows the detailed features of Fig. 9. It is found that the best performance is provide by the Scenario 5 (proposed control method), indicated by smallest overshoot and fastest settling time.

In dynamic stability study, the balance between electrical power from the excitation system and mechanical power from turbine is essential. In the electrical power excitation system is play important role to give magnetic flux in the rotor of the generator. In the dynamic study the input of excitation system is summation between voltage reference and power plant voltage. Hence it is essential to make the voltage of the power plant have a minimum overshoot and fastest settling time so that error between reference voltage and real plant voltage is small. Similar with the rotor speed and rotor angle results, in the voltage's non-linear time domain response, the best response is provided by the proposed method (Scenario 5) as depicted in Figure 10. As shown in Figure 10, the proposed method provides the smallest overshoot and the fastest settling time compared to
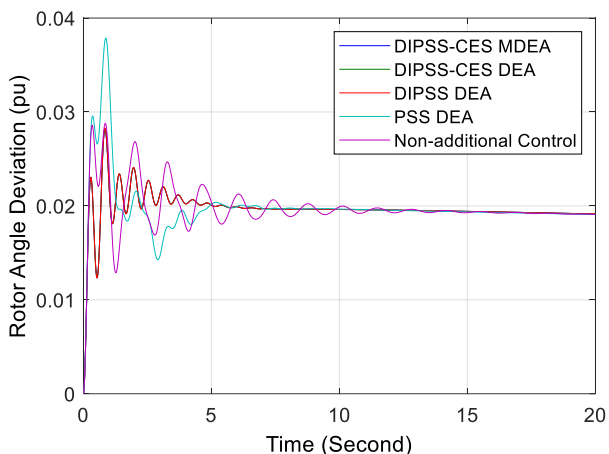
Figure. 9 Rotor angle changes in Suralaya power plant

Table 3. Detailed features of Figure. 9

Index	Scena rio 1	Scena rio 2	Scena rio 3	Scena rio 4	Scen ario 5
Oversh oot	0.0286	0.029 6	0.023 1	0.023 1	0.02 30
Settlin g time	>10	8.6	7.2	7.2	7.2
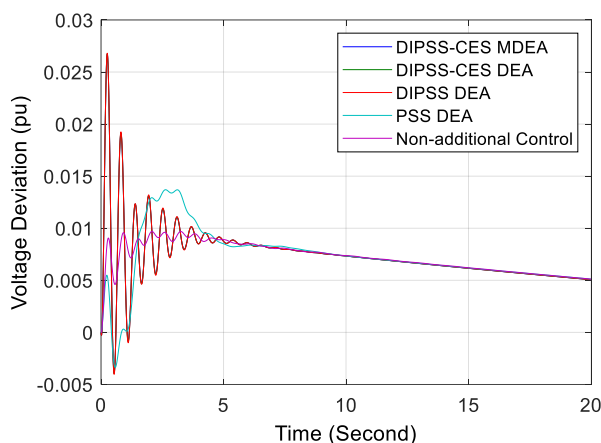
Figure. 10 Voltage changes in Suralaya power plant

the other scenarios. As shown in Fig. 8, 9 and 10, the proposed controlled method is provided the best performance compared to the other scenarios. Furthermore, to validate this result, calculating the total kinetic energy is essential.

4.2 Case study 2

In the case study 2, the focus is on investigating the transient kinetic energy (TKE) on the power plant [27]. The TKE assessment is used to investigated how much mechanical energy have been used by some system in the transient condition. In this study the smaller the value the less the mechanical energy has been used. The mathematical calculation of TKE can be described using Eq. (50).

Table 4. TKE value under different scenarios

In de x	Scenario 1	Scenar io 2	Scenar io 3	Scenar io 4	Scenar io 5
T K E	0.00000 1102667 4	0.0000 00473 9	0.0000 00408 2	0.0000 00408 0	0.0000 00407 6

$$TKE = \sum_{i=1}^{n} \frac{1}{2} J_i \cdot \Delta \omega_i^2 \qquad (50)$$

In Eq. (4), the angular momentum of the rotor at synchronous speed and speed deviation of ith generator in a system with n machines are described as J_i and $\Delta \omega_i$. Table 4 shows the TKE value comparison of Suralaya power plant under different scenarios. It is noticeable that the TKE value for Suralaya power plant is the smallest one when proposed controller method is added to the system.

5. Conclusions

This paper focused on designing coordinated control between dual input power system stabilizer and capacitor energy storage using modified differential evolution algorithm. From the simulation results it is found that low frequency oscillation can be damp by using CES and DIPSS. In addition, MDEA can be a smart solution to design the parameter of CES and DIPSS this is indicated by all the dynamic response of the system giving a better result compared to the other scenarios. Moreover, for further research the present of renewable based power plant in the system can be considered.

Conflicts of Interest

"The authors declare no conflict of interest."

Author Contributions

"Conceptualization, Akbar Swandaru, Muhammad Abdillah and Herlambang Setiadi; methodology, Akbar Swandaru, and Dimas Anton Asfani; Akbar Swandaru, Herlambang Setiadi and Tigor Hamonangan Nasution; validation, Akbar Swandaru, Muhammad Abdillah and Herlambang Setiadi; formal analysis, Akbar Swandaru, and Dimas Anton Asfani; investigation, Akbar Swandaru, Awan Uji Krismanto and Tigor Hamonangan Nasution; resources, Akbar Swandaru; writing original draft preparation, Akbar Swandaru; writing review and editing, Muhammad Abdillah, Awan Uji Krismanto, and Herlambang Setiadi; visualization, Akbar Swandaru, Tigor Hamonangan Nasution, and Dimas Anton Asfani. All authors have read and agreed to the published version of the manuscript".

Acknowledgment

Appendix

Table 5. List of annotation

Symbol	Meaning
K_1, K_2, K_4, K_5, K_6	The functions of the operating real and reactive loading as well as the excitation levels in the generator
C_3	A function of ratio of impedance
K_A	Amplifier gain
K_E	Exciter gain
K_F	Filter gain
K_{gw}	Gain of governor
$\dot{\delta}_i$	Rotor angle
M	2x *Inertia constant*
R_e	Equivalent resistance of transmission line
T_A	Time constant of amplifier
T_E	Time constant of exciter
T_F	Time constant of filter
T_{gu}	Time constant of governor
T_r	Time constant of transducer
t_{sim}	The time simulation
T_{tu}	Time constant of turbine
T_w	Time constant for washout filter
T'_{do}	Time constant for generator field
X_e	Equivalent reactance of transmission line
Z_{eq}	Equivalent impedance
$\Delta E'_q$	Voltage generator deviation
ΔT_e	Electrical torque deviation
ΔT_G	Governor output deviation
ΔT_m	Mechanical torque deviation
ΔV_A	Voltage deviation of amplifier
ΔV_F	Voltage deviation of filter
ΔV_{FD}	Voltage field deviation
ΔV_{Le}	Voltage output of washout filter
ΔV_R	Transducer voltage deviation
ΔV_{REF}	Voltage reference
ΔV_t	Terminal voltage of generator
$\Delta \omega$	Rotor speed deviation

References

[1] M. Kanálik, A. Margitová, B. Dolník, D. Medveď, M. Pavlík, and J. Zbojovský, "Analysis of low-frequency oscillations of electrical quantities during a real black-start test in Slovakia", *Int. J. Electr. Power Energy Syst.*, Vol. 124, p. 106370, 2021.

[2] U. Markovic, O. Stanojev, P. Aristidou, E. Vrettos, D. S. Callaway, and G. Hug, "Understanding small-signal stability of low-inertia systems", *IEEE Trans. Power Syst.*, 2021.

[3] J. J. Kim and J. H. Park, "A Novel Structure of a Power System Stabilizer for Microgrids", *Energies*, Vol. 14, No. 4, p. 905, 2021.

[4] U. Akram and M. Khalid, "A Coordinated Frequency Regulation Framework Based on Hybrid Battery-Ultracapacitor Energy Storage Technologies", *IEEE Access*, Vol. 6, pp. 7310-7320, 2018.

[5] M. A. Sobhy, A. Y. Abdelaziz, H. M. Hasanien, and M. Ezzat, "Marine predators algorithm for load frequency control of modern interconnected power systems including renewable energy sources and energy storage units", *Ain Shams Eng. J.*, 2021.

[6] S. Oshnoei, A. Oshnoei, A. Mosallanejad, and F. Haghjoo, "Novel load frequency control scheme for an interconnected two-area power system including wind turbine generation and redox flow battery", *Int. J. Electr. Power Energy Syst.*, Vol. 130, p. 107033, 2021.

[7] M. Khasanov, S. Kamel, C. Rahmann, H. M. Hasanien, and A. A. Durra, "Optimal distributed generation and battery energy storage units integration in distribution systems considering power generation uncertainty", *IET Gener. Transm. Distrib.*, 2021.

[8] M. Mv, "Model-predictive control-based hybrid optimized load frequency control of multi-area power systems", *IET Gener. Transm. Distrib.*, Vol. 15, No. 9, pp. 1521-1537, 2021.

[9] S. Suresh and S. Lal, "Modified differential eVolution algorithm for contrast and brightness enhancement of satellite images", *Appl. Soft Comput.*, Vol. 61, No. Supplement C, pp. 622-641, 2017.

[10] V. Vittal, J. D. McCalley, P. M. Anderson, and A. A. Fouad, *Power system control and stability*. John Wiley & Sons, 2019.

[11] R. Devarapalli, B. Bhattacharyya, N. K. Sinha, and B. Dey, "Amended GWO approach based multi-machine power system stability enhancement", *ISA Trans.*, Vol. 109, pp. 152-174, 2021.

[12] A. Nateghi and H. Shahsavari, "Optimal Design of FPI^ λ D^ μ based Stabilizers in Hybrid Multi-Machine Power System Using GWO Algorithm", *J. Oper. Autom. Power Eng.*, Vol. 9, No. 1, pp. 23-33, 2021.

[13] I. Kamwa, R. Grondin, and G. Trudel, "IEEE PSS2B versus PSS4B: the limits of performance of modern power system stabilizers", *IEEE Trans. Power Syst.*, Vol. 20, No. 2, pp. 903-915, 2005.

[14] H. Setiadi, N. Mithulananthan, and R. Shah, "Simultaneous Parameter Optimization for Coordinated Control of BESS and DIPSS using Clonal Selection", In: *Proc. of 2018 IEEE PES Asia-Pacific Power and Energy Engineering Conference*, pp. 13-18, 2018.

[15] A. Sharma and M. L. Kothari, "Intelligent dual input power system stabilizer", *Electr. Power Syst. Res.*, Vol. 64, No. 3, pp. 257-267, 2003.

[16] M. R. Shakarami and I. F. Davoudkhani, "Wide-area power system stabilizer design based on Grey Wolf Optimization algorithm considering the time delay", *Electr. Power Syst. Res.*, Vol. 133, pp. 149-159, 2016.

[17] S. Paszek and A. Nocoń, "Parameter polyoptimization of PSS2A power system stabilizers operating in a multi-machine power system including the uncertainty of model parameters", *Appl. Math. Comput.*, Vol. 267, pp. 750-757, 2015.

[18] K. Singh, "Enhancement of frequency regulation in tidal turbine power plant using virtual inertia from capacitive energy storage system", *J. Energy Storage*, Vol. 35, p. 102332, 2021.

[19] D. Libao, W. Debao, Q. Liyan, B. Xiaolong, and Z. Baoquan, "Optimization of core-based SOC test scheduling based on modified differential eVolution algorithm", In: *Proc. of 2016 IEEE Autotestcon*, pp. 1-6, 2016.

[20] M. R. Nayak, K. R. Krishnanand, and P. K. Rout, "Modified differential eVolution optimization algorithm for multi-constraint optimal power flow", In: *Proc. of 2011 International Conference on Energy, Automation and Signal*, pp. 1-7, 2011.

[21] W. S. Sakr, R. A. E. Sehiemy, and A. M. Azmy, "Optimal allocation of TCSCs by adaptive DE algorithm", *IET Gener. Transm. Distrib.*, Vol. 10, No. 15, pp. 3844-3854, 2016.

[22] S. Wang, L. Yu, L. Wu, Y. Dong, and H. Wang, "An Improved Differential EVolution Algorithm for Optimal Location of Battery Swapping Stations Considering Multi-Type Electric Vehicle Scale EVolution", *IEEE Access*, Vol. 7, pp. 73020-73035, 2019.

[23] T. D. F. Araújo and W. Uturbey, "Performance assessment of PSO, DE and hybrid PSO–DE algorithms when applied to the dispatch of generation and demand", *Int. J. Electr. Power Energy Syst.*, Vol. 47, No. Supplement C, pp. 205-217, 2013.

[24] W. Deng, H. Liu, J. Xu, H. Zhao, and Y. Song, "An improved quantum-inspired differential eVolution algorithm for deep belief network", *IEEE Trans. Instrum. Meas.*, 2020.

[25] A. M. E. Zonkoly, A. A. Khalil, and N. M. Ahmied, "Optimal tunning of lead-lag and fuzzy logic power system stabilizers using particle swarm optimization", *Expert Syst. Appl.*, Vol. 36, No. 2, pp. 2097-2106, 2009.

[26] H. Setiadi, N. Mithulananthan, R. Shah, T. Raghunathan, and T. Jayabarathi, "Enabling resilient wide-area POD at BESS in Java, Indonesia 500 kV power grid", *IET Gener. Transm. Distrib.*, Vol. 13, No. 16, pp. 3734-3744, 2019.

[27] A. Sajadi, R. Preece, and J. V. Milanovic, "Establishment multidimensional transient stability boundaries for power systems with uncertainties", In: *Proc. of 2018 Power Systems Computation Conference*, pp. 1-8, 2018.